Journal of Organometallic Chemistry 949 (2021) 121933

Contents lists available at ScienceDirect

Journal of Organometallic Chemistry

journal homepage: www.elsevier.com/locate/jorganchem

Ruthenium–*p*-cymene complexes with acylthiourea, and its heterogenized form on graphene oxide act as catalysts for the synthesis of quinoxaline derivatives

Dharmalingam Sindhuja[a], Mayakrishnan Gopiraman[b], Punitharaj Vasanthakumar[a], Nattamai Bhuvanesh[c], Ramasamy Karvembu[a,*]

[a] Department of Chemistry, National Institute of Technology, Tiruchirappalli, Tamil Nadu 620015, India
[b] Department of Applied Bioscience, College of Life and Environmental Science, Konkuk University, 120 Neungdong-ro, Gwangjin-gu, Seoul 05029, South Korea
[c] Department of Chemistry, Texas A&M University, College Station, TX 77842, United States

ARTICLE INFO

Article history:
Received 1 March 2021
Revised 14 May 2021
Accepted 7 June 2021
Available online 11 June 2021

Keywords:
Ruthenium complexes
Acylthiourea ligand
Graphene oxide
Heterogeneous catalysis
Quinoxalines

ABSTRACT

Synthesis of a series of half-sandwich Ru(II) complexes (**1**-**5**) containing acylthiourea ligand is reported herein. All the Ru(II) complexes were well characterized by analytical and spectroscopic (UV-Vis, FT-IR, NMR and mass spectrometry) methods. Molecular structures of two (**2** and **3**) of the complexes were confirmed by single crystal X-ray diffraction, and the complexes adopted pseudo-octahedral geometry around Ru. Catalytic ability of the Ru complexes was evaluated in the synthesis of quinoxaline compounds from various 2-nitroaniline and hydroxy ketone derivatives *via* transfer hydrogenation approach. Active homogeneous catalyst was heterogenized by supporting it on graphene oxide, and the heterogeneous equivalent was characterized by Raman, XPS, TEM, SEM and ICP-OES techniques. Activity of the heterogeneous catalyst was tested, and it can be reused up to five cycles without any loss in activity.

1. Introduction

Quinoxalines or benzopyrazines are significant core units, acting as effective pharmacophores, imparting noticeable biological activities such as antibacterial, antiviral, anti-inflammatory, anticancer *etc*., which make them to be a part of many widely used therapeutic agents [1,2]. Molecules bearing quinoxaline motifs, such as varenicline, brimonidine, quinacillin, chloroquinoxaline sulphonamide, botryllazine B, riboflavin etc., are therapeutically significant (Fig. 1). Besides biological applications, quinoxalines have been used as a basic building block in preparing various dyes, semiconductors, luminescent materials, cavitands, chemically controllable switches, *etc* [3–8]. Synthetic methodologies widely used so far for preparing quinoxaline derivatives are reported by Xie *et al* [9]. However, simple and environmentally friendly procedures have received great attention for the past few years [10]. For this purpose, transfer hydrogenation strategy is very useful [11]. Ru compounds are established as active catalysts for transfer hydrogenation and acceptor-less dehydrogenation for the synthesis of heterocycles, *etc* [12–16]. In the recent past, various half-sandwich Ru-arene catalysts have been used in many useful organic transformations like intermolecular Markovnikov selective hydroacylation of olefins, biomass conversions, *N*-alkylation of amines, *etc* [17–19]. The arene ligand in Ru complexes is essential for restricting further oxidation of metal in octahedral complexes. Furthermore, preparation of half-sandwich Ru complexes is feasible under mild conditions in high yields with good purity, and they are soluble in many organic solvents [20]. Even though the homogeneous catalysts are highly active and selective, catalyst contamination is often seen in the final product due to the complications involved in the separation processes. On the other hand, heterogeneous catalysts overcome the problem of separation. To maintain the advantages of both homogeneous and heterogeneous systems, active complexes are anchored on a solid support such as silica, alumina, carbon materials *etc* [21–23]. Carbon materials are found to have good tensile strength, large surface area, promising thermal stability and an ability to be functionalized. Many noble metal catalysts were immobilized on carbon materials and used in various organic transformations and electrocatalysis. Graphene is the basic building block for carbon materials of different dimensionalities: fullerenes (0D), nanotubes (1D) or graphite (3D). Synthetic approach widely adopted for graphene is the chemical oxidation and exfoliation

* Corresponding author.
E-mail address: kar@nitt.edu (R. Karvembu).

https://doi.org/10.1016/j.jorganchem.2021.121933
0022-328X/

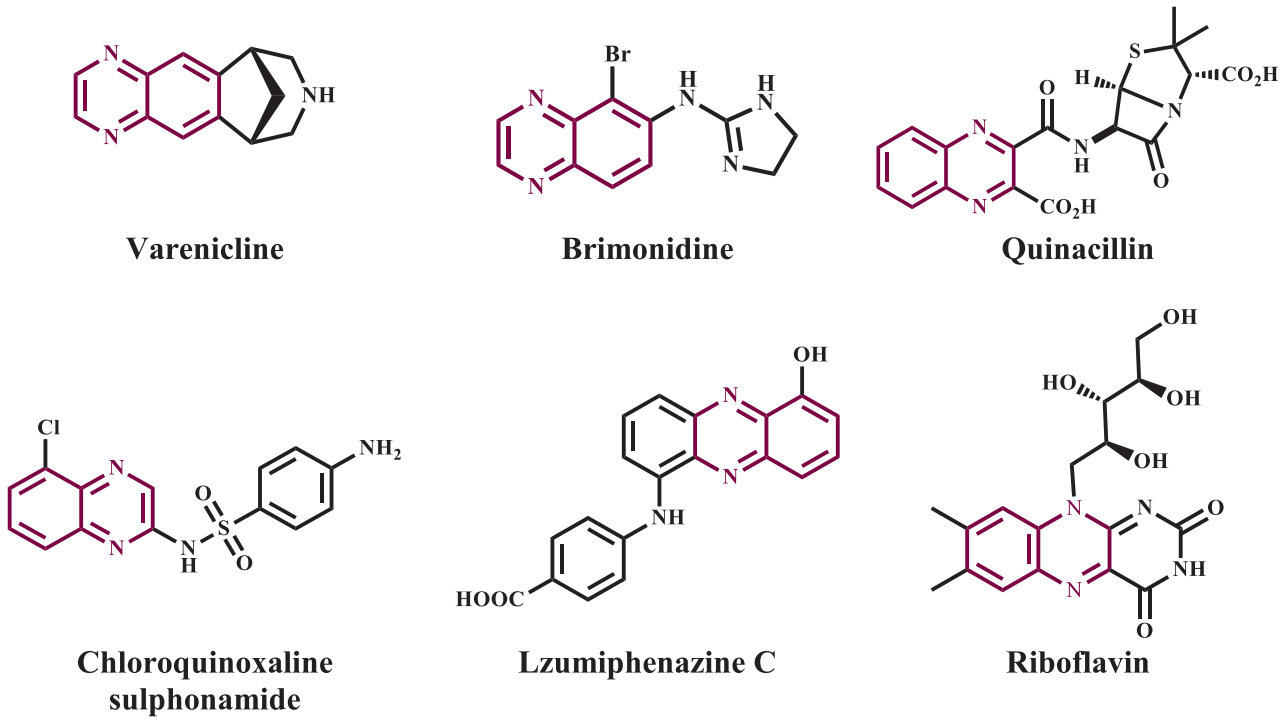

Fig. 1. Some bioactive molecules composing quinoxaline scaffold.

of graphite to graphene oxide (GO) followed by reduction. Importantly, graphene can be produced in a relatively larger scale. Moreover, its surface properties can be easily modified by introducing a variety of defects and oxygen-containing groups. Although the residual defects and oxygen-containing groups are detrimental to the electronic properties of graphene, they are important for other applications since the defects can play a role as anchoring sites and enhance the interaction with a second component [24–29]. Hence, graphene surface can be decorated with metal complexes or metal nanoparticles, and employed as catalysts for various reactions [30–34]. Recently, Peris and his co-workers reported the immobilization of Pd and Ru complexes on graphene surface through non-covalent interactions, and their catalytic activity was demonstrated in olefin reduction and dehydrogenation of alcohol [35]. The stable Ru-arene complexes containing graphene oxide supported chiral acylthiourea ligand were reported as catalysts for transfer hydrogenation of carbonyl compounds [36]. The stability and activity of these graphene-based Ru-arene complexes motivated us to develop analogues homogeneous and heterogeneous catalysts for one-pot quinoxaline synthesis from 2-nitroaniline and hydroxy ketone by implementing transfer hydrogenation approach.

2. Experimental section

Reagent grade chemicals were used without any further purification**.** The solvents were purified by standard procedures. Melting points were measured in open capillary tubes in a Sigma melting point apparatus. UV-visible spectra were recorded using a Shimadzu UV-2600 instrument. Fourier transform infrared (FT-IR) spectra were recorded as KBr pellets on Thermo Scientific Nicolet iS5 FT-IR spectrometer in the range of 550-4000 cm^{-1}. ^{1}H and ^{13}C nuclear magnetic resonance (NMR) spectra were recorded on a Bruker 500 MHz spectrometer in DMSO-d_6 or $CDCl_3$ with tetramethyl silane as an internal reference. Ruthenium was quantified by using PerkinElmer Optima 5300 DV inductively coupled optical emission spectrometer. X-ray photoelectron spectroscopic (XPS) analyses were done on a Kratos Axis-Ultra DLD instrument. During the analyses, samples were irradiated with Mg Kα X-ray source. The scanning electron microscopic (SEM) images were obtained by using a Bruker microscope. The transmission electron microscopic (TEM) images were seen by using a JEOL JEM 2100 microscope. Raman spectra were recorded by using a Bruker RFS 27 spectrometer. The quinoxaline derivatives were analyzed using Shimadzu GC 2010 and Shimadzu GCMS-QP2010 Ultra instruments equipped with a 60 m $\times$ 0.32 mm Restek Rtx-5 column.

2.1. Synthesis of the ligands

Ligands were synthesized according to the reported procedure. A solution of 2,4-dichlorobenzoyl chloride or cyclohexane carbonyl chloride in acetone (15 mL) was added dropwise to the suspension of potassium thiocyanate in acetone (15 mL) under stirring, and the solution was refluxed for an hour. The mixture was cooled to room temperature, and liquid NH_3 was added slowly. The reaction mixture was poured into 300 mL of deionised water, and the formed precipitate was collected by filtration. The ligands (L2 and L5) were washed with water and dried. Ligands L1, L3 and L4 were reported by us earlier [37,38].

N-carbamothioyl-2,4-dichlorobenzamide (L2): Yield: 78%. White solid. Mp: 169°C. UV-vis (CH_3CN): λ_{max} (nm) 203, 282. FT-IR (KBr, cm^{-1}): 3345 and 3151 (s; $\nu(NH_2)$), 3254 (s; ν(N–H)), 1688 (s; ν(C=O)), 1122 (s; ν(C=S)). ^{1}H NMR (500 MHz, DMSO-d_6): δ, ppm 11.64 (s, 1H), 9.60 (s, 1H), 7.91 (s, 1H), 7.73-7.51 (m, 3H). ^{13}C NMR (125 MHz, DMSO-d_6): δ, ppm 181.9, 167.7, 136.4, 134.7, 131, 130.5, 129.5, 127.7.

N-carbamothioylcyclohexanecarboxamide (L5): Yield: 82%. White solid. Mp: 164°C. UV-vis (CH_3CN): λ_{max} (nm) 208, 274. FT-IR (KBr, cm^{-1}): 3344 and 3194 (s; $\nu(NH_2)$), 3243 (s; ν(N–H)), 1693 (s; ν(C=O)), 1185 (s; ν(C=S)). ^{1}H NMR (500 MHz, DMSO-d_6): δ, ppm 10.91 (s, 1H), 9.59 (s, 1H), 9.25 (s, 1H), 2.48-2.34 (m, 1H), 1.66 (t, J = 14.6 Hz, 4H), 1.27-1.01 (m, 6H). ^{13}C NMR (125 MHz, DMSO-d_6): δ, ppm 182.4, 178.0, 44.2, 29, 25.6, 25.3.

2.2. Synthesis of the Ru complexes

A mixture of $[RuCl_2(\eta^6\text{-}p\text{-cymene})]_2$ (0.2 mmol, 122.4 mg) and ligand (L1-L5) (68-99 mg, 0.4 mmol) in toluene (30 mL) was stirred for 6-9 h at 27 °C. The reaction mixture was concentrated, and hexane was added to get orange coloured precipitate. The obtained complex was filtered, washed with hexane and diethyl ether, and dried *in vacuo*.

*[$RuCl_2(\eta^6$-p-cymene)L1] (**1**):* Yield: 92%. Orange solid. Mp: 238°C. UV-vis ($CHCl_3$): λ_{max} (nm) 279, 335, 434. FT-IR (KBr, cm^{-1}): 3353 and 3167 (s; $\nu(NH_2)$), 3237 (s; ν(N−H)), 1683 (s; ν(C=O)), 1112 (s; ν(C=S)). ^{1}H NMR (500 MHz, $CDCl_3$): δ, ppm 10.40 (s, 1H), 10.06 (s, 1H), 7.94 (s, 1H), 7.78 (d, J = 3.6 Hz, 1H), 7.63 (d, J = 1.0 Hz, 1H), 6.55 (dd, J = 3.6, 1.6 Hz, 1H), 5.45 (d, J = 5.9 Hz, 2H), 5.27 (d, J = 5.9 Hz, 2H), 3.14-2.94 (m, 1H), 2.28 (s, 3H), 1.35 (d, J = 6.9 Hz, 5H). ^{13}C NMR (126 MHz, $CDCl_3$): δ, ppm 180.8, 157.3, 147.6, 144.5, 121.3, 113.0, 103.6, 99.7, 84.1, 82.5, 30.5, 22.2, 18.3. ESI-MS (m/z): found 405.0174 $[M\text{-}2HCl+H]^+$ (calcd. 405.0210).

*[$RuCl_2(\eta^6$-p-cymene)L2] (**2**):* Yield: 70%. Orange solid. Mp: 164°C. UV-vis ($CHCl_3$): λ_{max} (nm) 254, 335, 432. FT-IR (KBr, cm^{-1}): 3342 and 3168 (s; $\nu(NH_2)$), 3238 (s; ν(N−H)), 1694 (s; ν(C=O)), 1107 (s; ν(C=S)). ^{1}H NMR (500 MHz, $CDCl_3$): δ, ppm 11.10 (s, 1H), 10.11 (s, 1H), 7.77 (s, 1H), 8.04 (d, J = 8.4 Hz, 1H), 7.43 (d, J = 2.0 Hz, 1H), 7.36 (dd, J = 8.4, 2.0 Hz, 1H), 5.42 (d, J = 5.9 Hz, 2H), 5.25 (d, J = 5.9 Hz, 2H), 3.03-2.95 (m, 1H), 2.26 (s, 3H), 1.33 (d, J = 6.9 Hz, 6H). ^{13}C NMR (126 MHz, $CDCl_3$): δ, ppm 181.8, 166, 139, 137.8, 133.5, 132.5, 130.7, 127.5, 83.9, 82.5, 30.5, 22.2, 18.3. ESI-MS (m/z): found 482.9532 $[M\text{-}2HCl+H]^+$ (calcd. 485.9636).

*[$RuCl_2(\eta^6$-p-cymene)L3] (**3**):* Yield: 85%. Orange solid. Mp.: 217°C. UV-vis ($CHCl_3$): λ_{max} (nm) 251, 336, 433. FT-IR (KBr, cm^{-1}): 3327 and 3197 (s; $\nu(NH_2)$), 3229 (s; ν(N−H)), 1682 (s; ν(C=O)), 1248 (s; ν(C=S)). ^{1}H NMR (500 MHz, DMSO-d_6): δ, ppm 11.18 (s, 1H), 9.79 (s, 1H), 9.50 (s, 1H), 7.86 (d, J = 7.4 Hz, 2H), 7.57 (t, J = 7.4 Hz, 1H), 7.44 (t, J = 7.8 Hz, 2H), 5.75 (d, J = 6.3 Hz, 2H), 5.71 (d, J = 6.2 Hz, 2H), 2.81-2.71 (m, 1H), 2.02 (s, 2H), 1.13 (d, J = 6.9 Hz, 6H). ^{13}C NMR (126 MHz, DMSO-d_6): δ, ppm 182.5, 168.2, 133.4, 129, 128.8, 106.8, 86.8, 85.9, 30.4, 21.9, 18.3. ESI-MS (m/z): found 415.1483 $[M\text{-}2HCl+H]^+$ (calcd. 415.0418).

*[$RuCl_2(\eta^6$-p-cymene)L4] (**4**):* Yield: 82%. Orange solid. Mp.: 252°C. UV-vis ($CHCl_3$): λ_{max} (nm) 253, 294, 342, 434. FT-IR (KBr, cm^{-1}): 3342 and 3164 (s; $\nu(NH_2)$), 3223 (s; ν(N−H)), 1665 (s; ν(C=O)), 1257 (s; ν(C=S)). ^{1}H NMR (500 MHz, $CDCl_3$): δ, ppm 11.02 (s, 1H), 10.21 (s, 1H), 8.43 (dd, J = 3.9, 1.0 Hz, 1H), 7.63 (dd, J = 5.0, 1.0 Hz, 1H), 7.16 (s, 1H), 7.13 (dd, J = 4.9, 4.0 Hz, 1H), 5.45 (d, J = 6.0 Hz, 2H), 5.28 (d, J = 6.0 Hz, 2H), 3.06-2.97 (m, 1H), 2.29 (s, 3H), 1.35 (d, J = 6.9 Hz, 6H). ^{13}C NMR (126 MHz, $CDCl_3$): δ, ppm 181.4 (C=S), 162.4 (C=O), 135.8, 135.4, 134.8, 129, 103.4, 99.8, 84.1, 82.5, 30.5, 22.2, 18.3. ESI-MS (m/z): found 421.9982 $[M\text{-}2HCl+H]^+$ (calcd. 421.0126).

*[$RuCl_2(\eta^6$-p-cymene)L5] (**5**):* Yield: 71%. Orange solid. Mp.: 172°C. UV-vis ($CHCl_3$): λ_{max} (nm) 279, 336, 439. FT-IR (KBr, cm^{-1}): 3341 and 3169 (s; $\nu(NH_2)$), 3243 (s; ν(N−H)), 1635 (s; ν(C=O)), 1161 (s; ν(C=S). ^{1}H NMR (500 MHz, $CDCl_3$): δ, ppm 10.68 (s, 1H), 9.99 (s, 1H), 7.67 (s, 1H), 5.43 (d, J = 5.6 Hz, 2H), 5.26 (d, J = 5.7 Hz, 2H), 3.02-2.97 (m, 1H), 2.26 (s, 3H), 1.91 (dd, J = 17.8, 6.5 Hz, 4H), 1.82-1.73 (m, 4H), 1.47-1.40 (m, 2H), 1.33 (d, J = 6.9 Hz, 6H). ^{13}C NMR (126 MHz, $CDCl_3$): δ, ppm 181.2, 178.4, 101.2, 96.7, 83.8, 82.4, 44.7, 30.5, 29.6, 25.4, 25, 22.2, 18.4. ESI-MS (m/z): found 420.0887 $[M\text{-}2HCl+H]^+$ (calcd. 421.0863).

2.3. Immobilization of Ru complex **4** on graphene oxide to get **6**

Steps involved in the immobilization are shown in Scheme 2. Graphene oxide was synthesized as per the modified Hummers method [39]. For further functionalization, graphene oxide (250 mg) was treated with excess thionyl chloride at 80 °C for 24 h to yield graphene oxide appended with acid chloride (GO-Cl). GO-Cl precipitate was washed thoroughly with diethyl ether and acetone to remove unreacted thionyl chloride, and dried under *vacuum* for 6 h. GO-Cl was modified by treating it (200 mg) with ligand L4 (2 mmol) in *N,N*-dimethylformamide (25 mL) at 100 °C for 24 h to get GO-L4 which was filtered, washed with ethanol and diethyl ether, and dried under *vacuum*. Ru−*p*-cymene dimer (1 mmol) dissolved in toluene (15 mL) was added to the dispersion of GO-L4 (200 mg) in toluene (15 mL), and the resulting mixture was stirred at room temperature for 10 h. The formed heterogeneous complex (**6**) was removed by means of filtration, and washed with toluene (3 × 10 mL) and hexane (3 × 10 mL) to remove the excess Ru−*p*-cymene dimer.

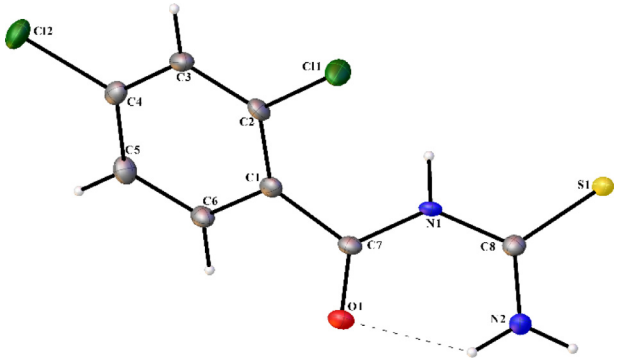

Fig. 2. Molecular structure of L2. Selected bond lengths (Å) and angles (°): C(7)−O(1) 1.219(3), C(8)−S(1) 1.689(2), N(1)−H(1) 0.88, N(2)−H(2A) 0.88, N(2)−H(2B) 0.88, S(1)−C(8)−N(1) 117.94(16), S(1)−C(8)−N(2) 123.37(17), N(2)−C(8)−N(1) 118.7(2), O(1) −C(7)−N(1) 123.9(2).

2.4. General procedure for the synthesis of quinoxaline derivatives

Initially, catalyst **4** (0.5 mol%) or **6** (0.5 mol%) and hydroxy ketone (benzoin / furoin / acetoin) were taken in formic acid / triethyl amine mixture (0.75 molar ratio), and stirred at 70 °C. 2-nitroaniline (or its derivative) was added to the above mixture, and the reaction was continued until nitroaniline was fully consumed (monitored by TLC). Then, the reaction mixture was diluted with water, and extracted with ethyl acetate. The combined organic layer was dried over anhydrous Na_2SO_4, filtered, and concentrated under *vacuum*. The crude was purified by column chromatography using hexane-ethyl acetate mixture (9:1) as eluent to afford pure quinoxaline derivative.

3. Results and discussion

3.1. Synthesis of the ligands

The ligands (L1-L5) were prepared by reacting corresponding acyl chlorides with potassium thiocyanate (1:1 stoichiometry) and liquid ammonia as per the reported procedure [37] and characterized by spectroscopic and analytical techniques. Ligands L2 and L5 were not yet reported, and hence they were crystallized to get single crystals.

3.2. Solid state structures of the ligands

Molecular structures of the ligands (L2 and L5) are shown in Figs. 2 and 3. Good quality crystals were grown from acetonitrile solutions of the ligands. The crystallographic and refinement parameters are summarized in Table S1. Ligands L2 and L5 crystallized in monoclinic (C12/*c*1) and triclinic (*P*-1) systems, respectively. C(7)−O(1) and C(8)−S(1) bond lengths were in the ranges of

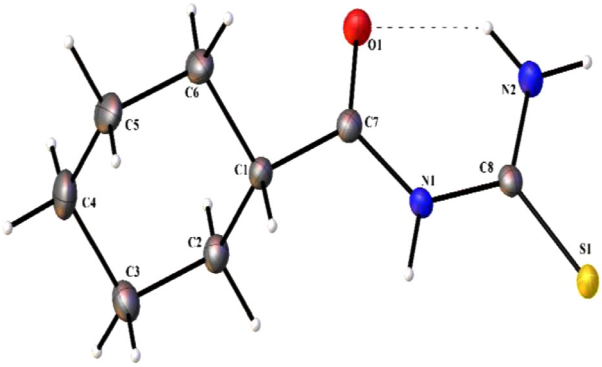

Fig. 3. Molecular structure of L5. Selected bond lengths (Å) and angles (°): C(7)–O(1) 1.2228(19), C(8)–S(1) 1.6843(16), N(1)–H(1) 0.88, N(2)–H(2A) 0.88, N(2)–H(2B) 0.88, S(1)–C(8)–N(1) 119.05(11), S(1)–C(8)–N(2) 123.24(12), N(2)–C(8)–N(1) 117.69(13), O(1)–C(7)–N(1) 122.57(14).

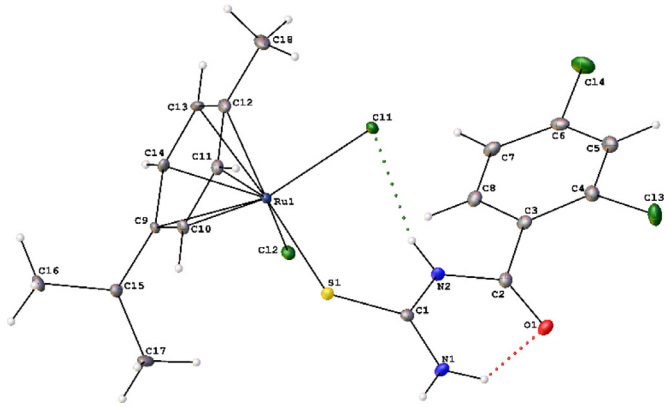

Fig. 4. Molecular structure of **2**. Selected bond lengths (Å) and angles (°): Ru(1)–Cl(1) 2.44465(9), Ru(1)–Cl(2) 2.4269(9), Ru(1)–S(1) 2.4079(10), S(1)–C(1) 1.691(4), O(1)–C(2) 1.218(5), N(1)–H(1A) 0.8800, N(2)–H(1A) 0.8800, N(2)–H(2) 0.8800, Cl(1)–Ru(1)–Cl(2) 87.49(3), Cl(1)–Ru(1)–S(1) 94.31(3), S(1)–Ru(1)–Cl(2) 89.39(3), C(1)–S(1)–Ru(1) 116.94(14), H(1A)–N(1)–H(1B) 120, C(1)–N(1)–H(1A) 120, C(1)–N(1)–H(1B) 120, C(1)–N(1)–H(2) 116.6, N(1)–C(1)–S(1) 120.7(3), N(1)–C(1)–N(2) 118.9(3), N(2)–C(1)–S(1) 120.1(3), O(1)–C(2)–N(2) 123.5(4).

1.219(3)-1.2228(19) and 1.689(2)-1.6843(16) Å, respectively [37,38]. N(1)–H(1), N(1)–H(2A) and N(1)–H(2B) bond lengths in L2 and L5 were fixed to be 0.88, 0.88 and 0.88 Å, respectively [37,40]. Two intramolecular hydrogen bonding interactions [N(2)–H(2A)…O(1), 1.98-2.04 Å and N(2)–H(2B)…S(1), 2.62-2.66 Å] were noted in both the ligands.

3.3. Synthesis and characterization of the Ru(II) complexes

Five Ru–*p*-cymene complexes (**1**-**5**) were synthesized by the treatment of one equivalent of $[RuCl_2(\eta^6\text{-}p\text{-cymene})]_2$ with two equivalents of corresponding acylthiourea ligands (L1-L5) in toluene at room temperature for 6-9 h (Scheme 1). The complexes were orange coloured, soluble in chloroform, acetonitrile, dichloromethane, dimethyl sulfoxide, dimethylacetamide and dimethylformamide, and less soluble in diethyl ether, hexane and water.

FT-IR spectra of the complexes showed stretching frequencies of NH_2 and N–H moieties in the ranges of 3164-3353 and 3223-3238 cm^{-1}, respectively. Similarly, carbonyl and thiocarbonyl stretching frequencies were observed at 1107-1257 and 1635-1694 cm^{-1}, respectively. Stretching frequencies of NH_2, N–H and C=O were almost unaltered when compared to those of the free ligands. But there was a decrease in C=S stretching frequency on complexation, which indicated the coordination of neutral S atom of the

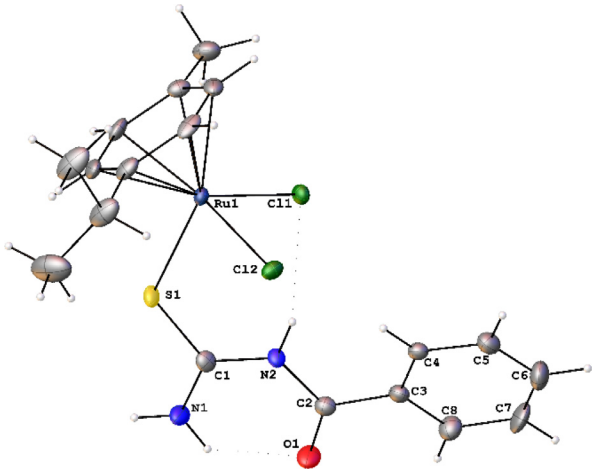

Fig. 5. Molecular structure of **3**. Selected bond lengths (Å) and angles (°): Ru(1)–Cl(1) 2.4193(4), Ru(1)–Cl(2) 2.4268(12), Ru(1)–S(1) 2.4136(12), S(1)–C(1) 1.711(5), O(1)–C(2) 1.226(6), N(1)–H(1A) 0.8800, N(2)–H(1A) 0.8800, N(2)–H(2) 0.8800, Cl(1)–Ru(1)–Cl(2) 85.845(5), Cl(1)–Cu(1)–S(1) 92.19(4), S(1)–Ru(1)–Cl(2) 91.65(4), C(1)–S(1)–Ru(1) 118.88(17), H(1A)–N(1)–H(1B) 120, C(1)–N(1)–H(1A) 120, C(1)–N(1)–H(1B) 120, N(1)–C(1)–S(1) 119.4(4), N(1)–C(1)–N(2) 119.5(4), N(2)–C(1)–S(1) 121.1(3), O(1)–C(2)–N(2) 122.0(4).

ligands to Ru. ^1H NMR spectra of the complexes displayed signals corresponding to N–H and NH_2 protons as singlets at 10.48-11.18 and 7.16-10.21 ppm, respectively. In addition to the signals due to acylthiourea protons, new signals observed in the regions 5.25-5.75 (two doublets), 2.02-2.29 (singlet), 2.76-3.02 (multiplet) and 1.13-1.35 (doublet) ppm were assigned to *p*-cymene ring, methyl, isopropyl methine and isopropyl methyl protons, respectively. ^{13}C NMR spectra of the complexes revealed the presence of thiocarbonyl (180.8-182.5 ppm) and carbonyl carbons (157.3-178.4 ppm), along with aromatic carbons of the ligands. The *p*-cymene ring carbons resonated in the region 82.4-106.8 ppm, and the aliphatic carbons gave signals in the region 18.3-30.5 ppm.

3.4. Solid state structures of the complexes

Single crystals of complexes **2** and **3** were obtained by slow evaporation of chloroform/acetonitrile solutions of the complexes. Molecular structures of the complexes are displayed in Figs. 4 and 5. A summary of crystallographic data, selected bond lengths and hydrogen bonding interactions are given in Table S2. Crystal system of complexes **2** and **3** was found to be monoclinic and orthorhombic, with $P121/c1$ and $Pna2_1$ space groups, respectively. Ru occupied the centre of pseudo-octahedron, with two chloride, one acylthiourea and one *p*-cymene ligands. *p*-Cymene occupied three coordination sites of Ru, leading to half-sandwich piano-stool structure. The acylthiourea ligands coordinated to Ru through S atom, and Ru–S bond length was measured as 2.4079(10) and 2.4136(12) Å in **2** and **3**, respectively, which is in accordance with the earlier reports [40–42]. Moreover, C=S bond length in the complexes was greater than that in the ligands. Also, intramolecular hydrogen bonding interactions of the type N(2)–H(2)…Cl(1) (2.32-2.499 Å) and N(1)–H(1A)…O(1) (1.946-2.01 Å) were seen in both the complexes. Ru–*p*-cymene centroid distance in **2** and **3** was found to be 1.661 and 1.662 Å, respectively.

3.5. Synthesis of quinoxaline derivatives from 2-nitroaniline and hydroxy ketone

3.5.1. Optimization of the reaction conditions

The reaction conditions were optimized by taking 2-nitroaniline and benzoin as substrates. Initially, the molar ratio of 2-

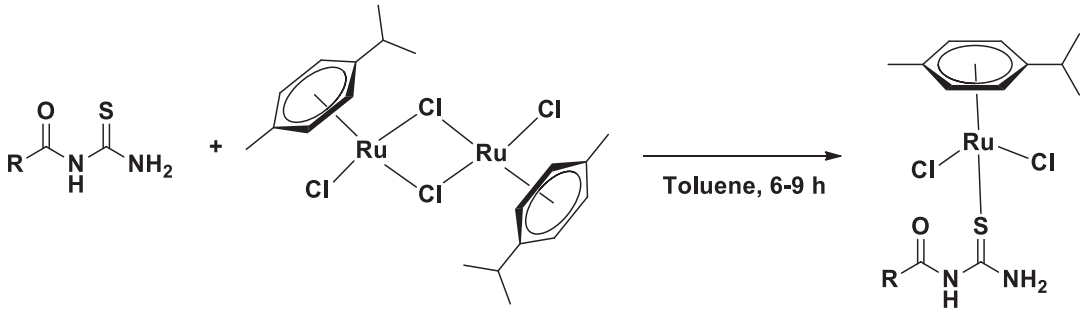

R					
Complex	1	2	3	4	5

Scheme 1. Synthesis of the Ru complexes.

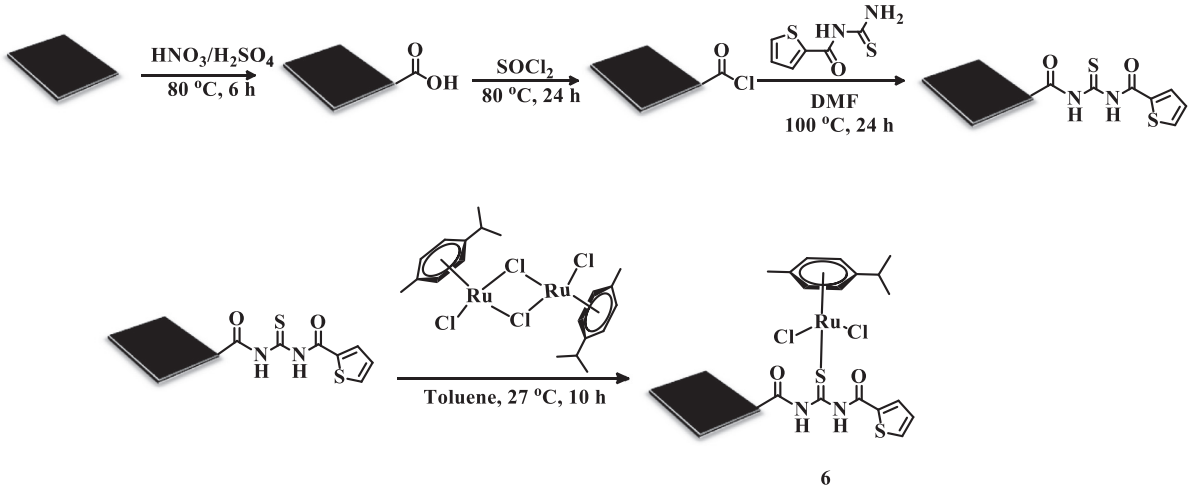

Scheme 2. Synthesis of the Ru complex supported on graphene oxide.

nitroaniline and benzoin was varied from 0.2 to 0.5, and complete conversion of 2-nitroaniline was obtained in 0.3 molar ratio. Influence of temperature on the conversion was investigated, and complete conversion was attained at 70 °C. Among the five complexes, complex **4** showed better activity with an isolated yield of 83% of 2,3-diphenylquinoxaline. Hence, complex **4** was used further for extending scope of the substrates. Since the use of 2-propanol as hydrogen donor/solvent did not lead to product formation, formic acid/triethyl amine system was used. The molar ratio of formic acid/triethyl amine was varied from 0.25 to 1.5; quantitative conversion (>99%) was achieved while using 0.75 molar ratio. Fixing the molar ratio of formic acid/triethyl amine as 0.75, catalyst amount and time were varied. Good conversion of 2-nitroaniline was observed with 0.5 mol% of the catalyst in 8 h. Control experiments were performed to establish the catalyst role; no conversion was observed in the absence of the catalyst or hydrogen donor. Also, the reaction did not proceed in the presence of Ru–*p*-cymene dimer. These results elucidated the role of Ru–*p*-cymene complex of acylthiourea in catalytic transfer hydrogenation.

*3.5.2. Catalytic performance by complex **4***

Table 1 summarizes the results of reactions between various 2-nitroaniline compounds and benzoin. Complex **4** catalyzed the conversion of 2-nitroaniline and benzoin into 2,3-diphenyl quinoxaline (**9a**) in 8 h with the yield of 83%. Catalytic efficiency was tested with electron releasing or electron withdrawing substituent in the substrates. 6-methoxy-2,3-diphenylquinoxaline (**9b**) and 6,7-dimethyl-2,3-diphenylquinoxaline (**9c**) were obtained in 66 and 68% yields, respectively. When nitroaniline with methyl group was employed, the reaction did not complete even after 24 h, and the maximum conversion was 54% with 100% selectivity (**9d**). Similarly, nitroaniline derivatives with halide (Br and Cl) were studied. 4-bromonitroaniline was coupled with benzoin to give 6-bromo-2,3-diphenylquinoxaline (**9e**) selectively (100%) with 87% conversion. The conversion (99%) was excellent in the case of chloro substituted nitroaniline, and the formation of 5-chloro-2,3-diphenylquinoxaline (**9f**) was observed with 100% selectivity. Also, reaction between nitroaniline (with trifluoromethyl substituent) and benzoin completed in 3 h with the selective formation of 2,3-diphenyl-6-(trifluoromethyl)quinoxaline (**9g**). Nitroani-

Table 1
Synthesis of quinoxaline derivatives from benzoin using catalyst **4**[a,b,c].

7 **8** **9**

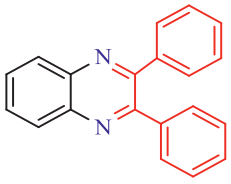

9a, 8 h, 83%[b]

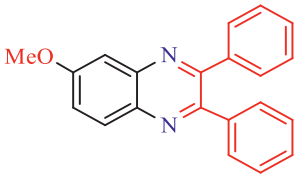

9b, 15 h, 66%[b]

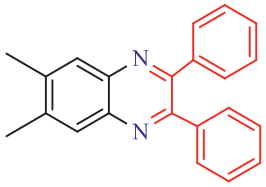

9c, 24 h, 68%[b]

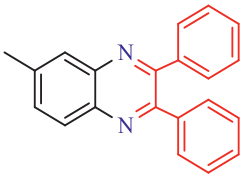

9d, 24 h, 54/>99%[c]

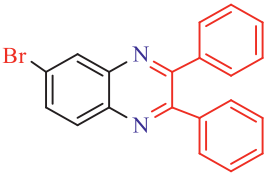

9e, 15 h, 87/>99%[c]

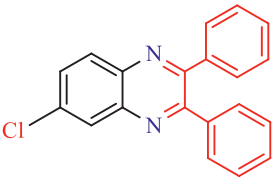

9f, 15 h, 99/>99%[c]

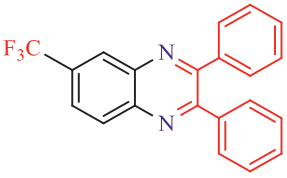

9g, 3 h, 99/>99%[c]

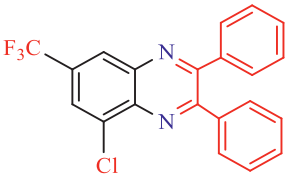

9h, 2 h, 99/>99%[c]

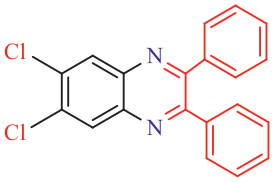

9i, 16 h, 77/>99%[c]

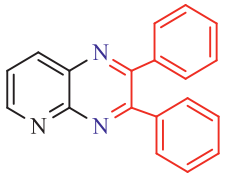

9j, 15 h, 99/>99%[c]

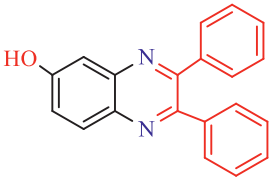

9k, 24 h, 99/>99%[c]

[a] Reaction conditions: **7** (0.5 mmol), **8** (1.4 mmol), **4** (0.5 mol%), $HCOOH/NEt_3$ (0.75 molar ratio), 70 °C.
[b] Isolated yield.
[c] Conversion/selectivity determined by GC-MS.

line with both trifluoromethyl and chloro substituents was used to produce 5-chloro-2,3-diphenyl-7-(trifluoromethyl)quinoxaline (**9h**) quantitatively in 2 h. 4,5-dichloro-2-nitroaniline was reacted with benzoin to give 6,7-dichloro-2,3-diphenylquinoxaline (**9i**). 2,3-diphenylpyrido[2,3-b]pyrazine (**9j**) and 2,3-diphenylquinoxaline-6-ol (**9k**) were formed with 100% selectivity.

Scope of the catalytic system was extended to the coupling of nitroaniline derivatives with 2,2'-furoin, and the details are provided in Table 2. All the nitroaniline substrates were smoothly combined with 2,2'-furoin in presence of catalyst **4**, and the products were obtained in 65-81% yields. Reaction of 2,2'-furoin with 2-nitroaniline or 4-methyl-2-nitroaniline gave 2,3-di(furan-2-yl)quinoxaline (**11a**) or 2,3-di(furan-2-yl)-6-methylquinoxaline (**11b**), respectively with excellent conversion and selectivity. Coupling of trifluoromethyl substituted nitroaniline with 2,2'-furoin yielded 2,3-di(furan-2-yl)-6-trifluoromethyl-quinoxaline (81%) (**11c**). Likewise, the yields of 5-chloro-2,3-di(furan-2-yl)-7-trifluoromethyl-quinoxaline (**11d**), 6-chloro-2,3-di(furan-2-yl)quinoxaline (**11e**) and 6-bromo-2,3-di(furan-2-yl)quinoxaline (**11f**) were 79, 65 and 72%, respectively.

Less reactive aliphatic hydroxy ketone (acetoin) was employed in the same reaction, and the details of conversions and selectivi-

Table 2
Synthesis of quinoxaline derivatives from furoin using catalyst **4**[a,b,c].

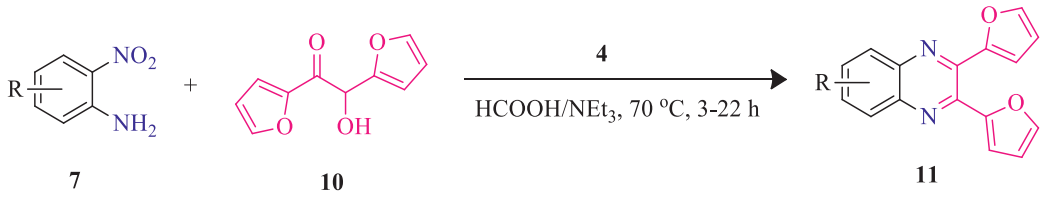

7 **10** **11**

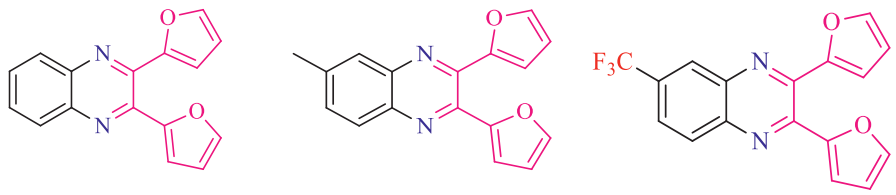

11a, 15 h, 99/>99%[b] **11b**, 22 h, 94/>99%[b] **11c**, 3 h, 81%[c]

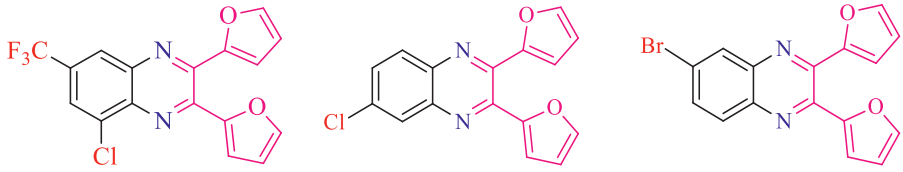

11d, 3 h, 79%[c] **11e**, 16 h, 65%[c] **11f**, 15 h, 72%[c]

[a] Reaction conditions: **7** (0.5 mmol), **10** (1.4 mmol), **4** (0.5 mol%), HCOOH/NEt_3 (0.75 molar ratio), 70 °C.
[b] Conversion/selectivity determined by GC-MS.
[c] Isolated yield.

Table 3
Synthesis of quinoxaline derivatives from acetoin using catalyst **4**[a,b].

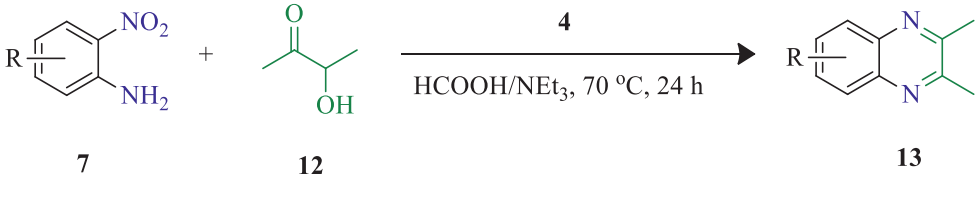

7 **12** **13**

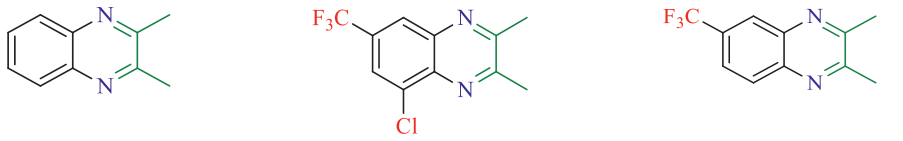

13a, 24 h, 99/>99% [b] **13b**, 24 h, 99/>99% [b] **13c**, 24 h, 69/>99% [b]

[a] Reaction conditions: **7** (0.5 mmol), **12** (1.4 mmol), **4** (0.5 mol%), HCOOH/NEt_3 (0.75 molar ratio), 70 °C.
[b] Conversion/selectivity determined by GC-MS.

ties are listed in Table 3. The reaction was slower compared to that with the other hydroxy ketones. Selectivity of quinoxaline derivatives was maintained in all the reactions. 2,3-dimethylquinoxaline (**13a**) and 5-chloro-2,3-dimethyl-7-(trifluoromethyl) quinoxaline (**13b**) were obtained with 99% conversion. The conversion of 2-nitro-5-(trifluoromethyl)aniline was only 69% with the selective formation of 2,3-dimethyl-6-(trifluoromethyl)quinoxaline (**13c**).

*3.6. Synthesis and characterization of the graphene supported Ru catalyst (**6**)*

Active Ru−*p*-cymene complex was supported on graphene oxide (**6**) as shown in Scheme 2. The morphology of graphene in **6** was observed by TEM and SEM as presented in Fig. 6 and S17 respectively, which showed the presence of graphene layers. SEM-EDAX spectrum (Fig. S17) confirmed the presence of various elements in the catalyst. TEM images of the catalyst revealed the layered structure of graphene, which also established the fact that the morphology of graphene oxide was unaltered even after complexation. In addition, Raman analysis provided the structural characteristics and properties of the graphene oxide support. The G line is usually assigned to the first order scattering of the E_{2g} phonons of sp^2 C atoms. The D line is the breathing mode of the *j*-point phonons of A_{1g} symmetry [43–45]. Raman spectrum (Fig. S16) of **6** showed two bands *i.e.*, D band at 1375 and G band at 1595 cm^{-1}. The relative intensity ratio is ~1.3 which was due to the increase

Table 4
Synthesis of quinoxaline derivatives from benzoin/furoin using heterogenized catalyst **6**[a,b].

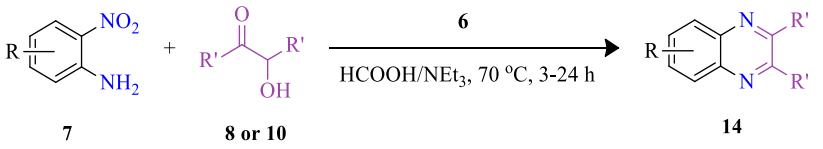

7 **8 or 10** **14**

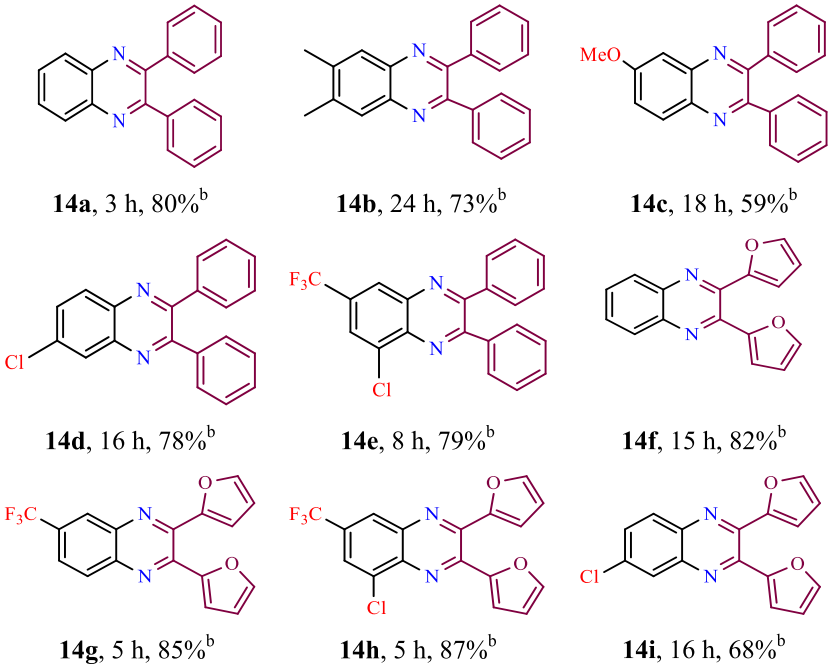

14a, 3 h, 80%[b] **14b**, 24 h, 73%[b] **14c**, 18 h, 59%[b]

14d, 16 h, 78%[b] **14e**, 8 h, 79%[b] **14f**, 15 h, 82%[b]

14g, 5 h, 85%[b] **14h**, 5 h, 87%[b] **14i**, 16 h, 68%[b]

[a] Reaction conditions: **7** (0.5 mmol), **8** or **10** (1.4 mmol), **6** (0.15 mol%), HCOOH/NEt_3 (0.75 molar ratio), 70 °C.
[b] Isolated yield.

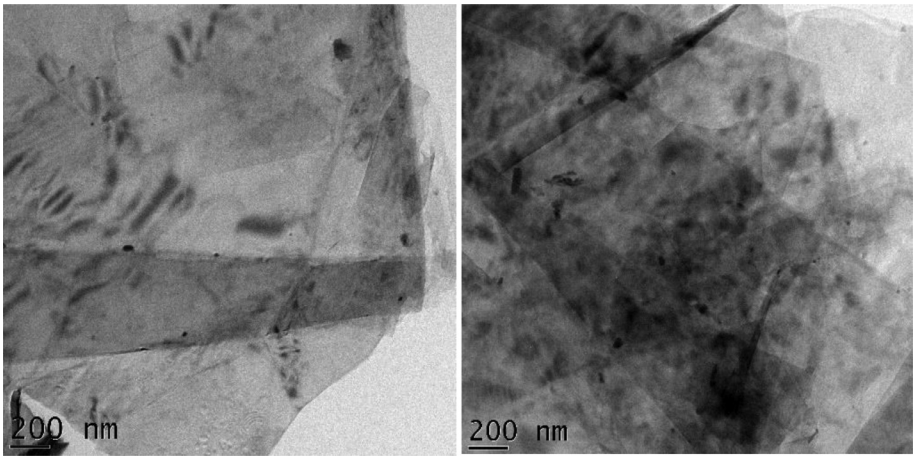

Fig. 6. TEM images of **6**.

in the degree of disorder. The disorder nature was due to the interaction between Ru complex and graphene oxide, which in turn confirmed the anchoring of Ru complex on graphene. XPS analyses were done to elucidate the chemical nature of the catalyst and the spectrum is shown in Fig. 7. The spectrum showed the presence of elements like Ru, O, S, N and Cl in **6**. The signals at 464.1 and 486.1 eV can be attributed to Ru $3p_{3/2}$ and Ru $3p_{1/2}$ core levels, respectively. The signal around 280 eV appeared as partially overlapped (C 1s and Ru 3d). Hence, Ru 3p levels were focussed primarily to confirm the presence of Ru. Furthermore, the Ru 3p core level peaks were best fitted to elucidate the +2 oxidation state of Ru in **6** [20,44]. The binding energies corresponding to Ru(0) and RuO_2 were not observed in Fig. 7, which confirmed that Ru loaded was only in the form of complex. XPS spectrum of **6** also possessed peaks due to N 1s, O 1s, S 2p and Cl 2p. ICP-MS study established 3.1 wt% loading of Ru over graphene oxide.

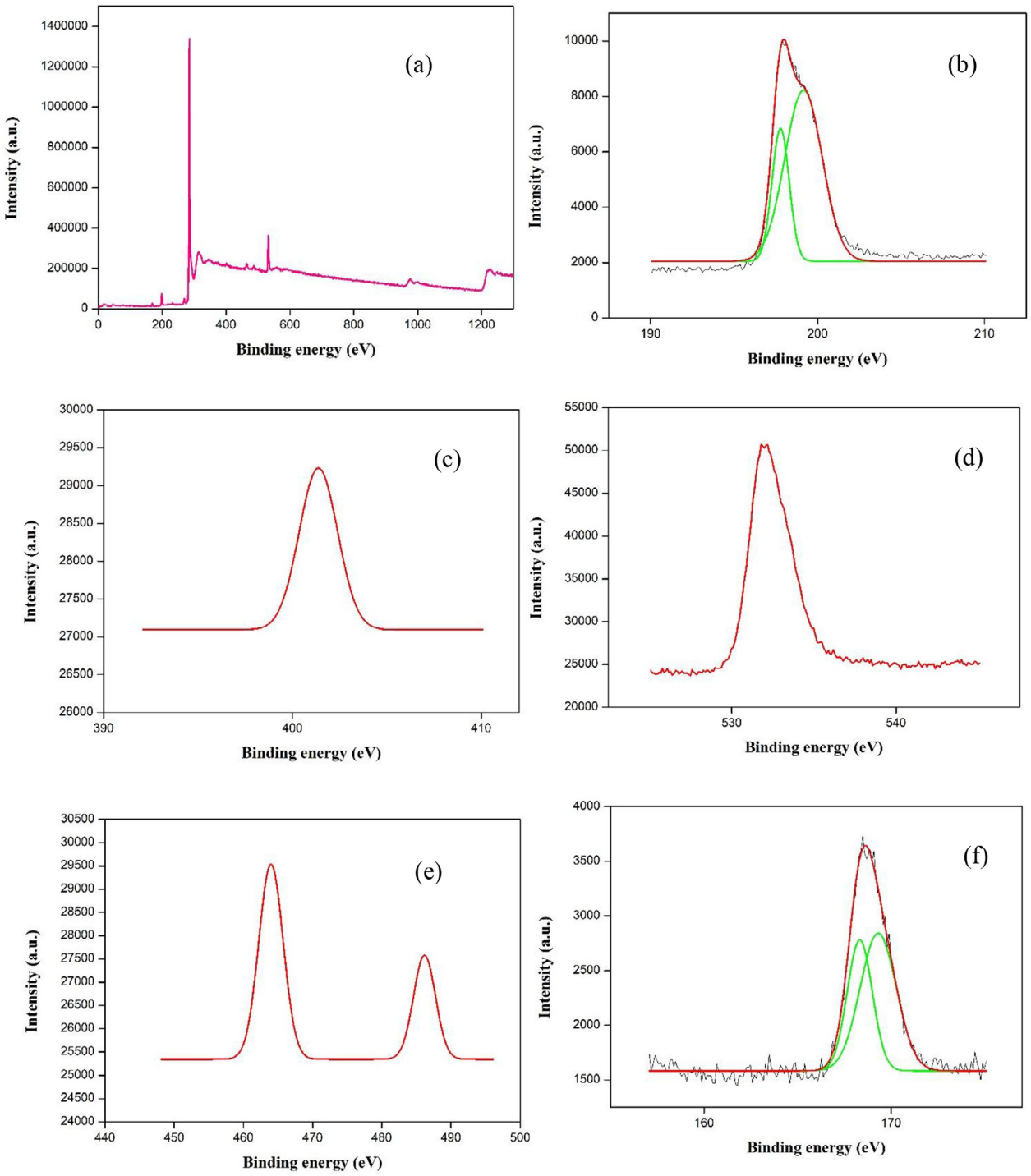

Fig. 7. XPS spectra (a) wide spectrum of **6** (b) Cl2p region (c) N1s region (d) O1s region (e) Ru3p region and (f) S2p region.

*3.7. Performance by catalyst **6***

Optimum catalyst loading was found by varying the amount of the catalyst in the reaction between 2-nitroaniline and benzoin, and good conversion of 2-nitroaniline was observed when it was 0.15 mol%. With the same optimum conditions, scope was extended. Catalyst **6** was used for the coupling of various 2-nitroaniline derivatives with benzoin / furoin, and the yields of the isolated products are summarized in Table 4. All the substrates were coupled smoothly in the presence of **6** to give the corresponding products in moderate to good yields. The present catalytic system yielded 2,3-diphenylquinoxaline (**14a**) from 2-nitroaniline and benzoin in 80% yield. Similarly, yields of 6,7-dimethyl-2,3-diphenylquinoxaline (**14b**) and 6-methoxy-2,3-diphenylquinoxaline (**14c**) were found to be 73 and 59%, respectively. Further, 78% of 5-chloro-2,3-diphenylquinoxaline (**14d**) was obtained in 12 h, and the yield was comparable with that obtained from carbon nanotube-Au nanohybrid catalytic system [46]. Also, yield of 5-chloro-2,3-diphenyl-7-(trifluoromethyl)quinoxaline (**14e**) was 79%. Like benzoin, 2,2'-furoin was also coupled with

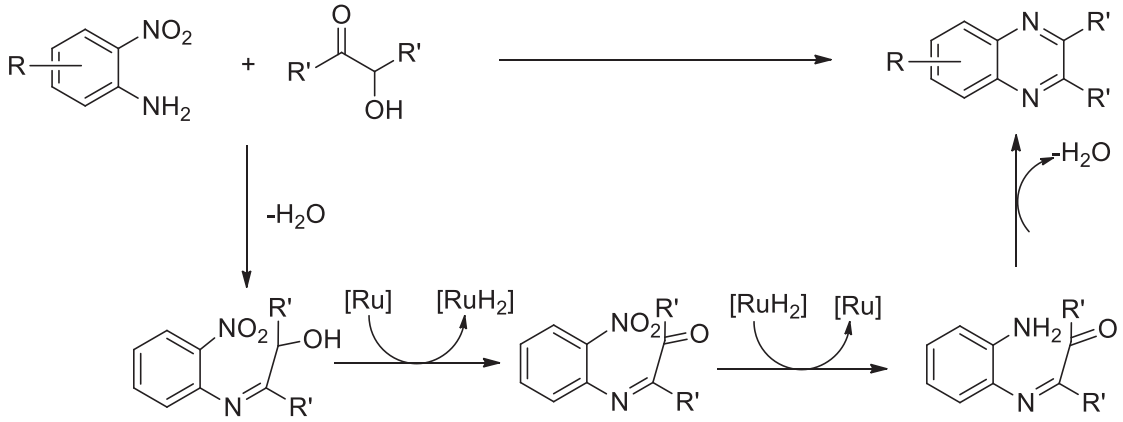

Fig. 8. Possible pathway for the synthesis of quinoxaline derivatives.

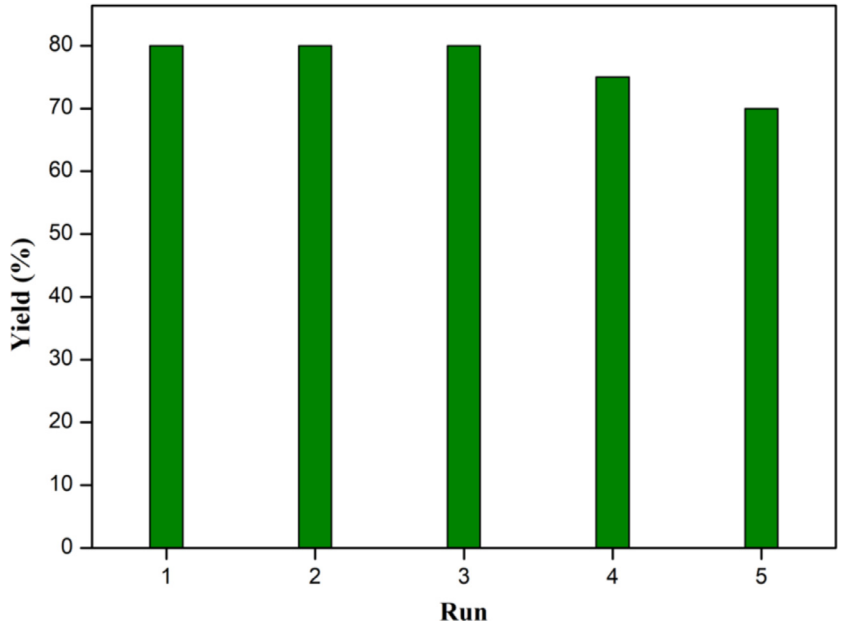

Fig. 9. Reusability of **6**.

various 2-nitroaniline derivatives to produce quinoxaline derivatives. The yields of 2,3-di(furan-yl)quinoxaline (**14f**), 2,3-di(furan-2-yl)-6-trifluoromethyl-quinoxaline (**14g**), 5-chloro-2,3-di(furan-2-yl)-7-trifluoromethyl-quinoxaline (**14h**) and 6-chloro-2,3-di(furan-2-yl)quinoxaline (**14i**) were 82, 85, 87 and 68%, respectively. Interestingly, this catalytic system is compatible for the substrates having electron withdrawing or electron donating substituent(s).

From GC and GC-MS analyses, it was found that there was no formation of diamine from 2-nitroaniline, which confirmed that the first step was imine formation, followed by transfer hydrogenation and cyclization. The possible pathway for quinoxaline formation is shown in Fig. 8.

*3.7.1. Reusability of the heterogenized catalyst (**6**)*

Catalyst **6** was used for the next cycle after washing it with water, ethanol and diethyl ether. Benzoin and 2-nitroaniline were used as substrates for the reusability tests. The reactions were carried out under the same optimized conditions. The yield of 2,3-diphenylquinoxaline was noted as 80% in the first run, and there was a little reduction in the yields after the third cycle. Catalyst was reused up to five cycles (Fig. 9).

4. Conclusions

Synthesis and characterization of air-stable half-sandwich Ru(II) complexes (**1**-**5**) are reported. Crystal structures of complexes **2** and **3** are described. Catalytic efficacy of **4** was better towards the synthesis of quinoxaline derivatives. Hence, it was made heterogeneous (**6**) by immobilizing it on graphene oxide and characterized. Scope of both homogeneous (**4**) and heterogeneous (**6**) catalysts has been extended to various 2-nitroaniline and hydroxy ketone derivatives. The present system has been proven to be versatile and efficient for the synthesis of quinoxaline derivatives. Also, heterogenous catalyst **6** is recyclable and it can be reused up to five cycles with good activity.

Declaration of Competing Interest

The authors declare no conflict of interest

Acknowledgement

We thank DAE-BRNS (34/14/52/2014-BRNS/2069) for financial support.

Supplementary materials

Supplementary material associated with this article can be found, in the online version, at doi:10.1016/j.jorganchem.2021.121933.

References

[1] T. Mathew, A. Papp, F. Paknia, S. Fustero, G.K. Surya Prakash, Benzodiazines: recent synthetic advances, Chem. Soc. Rev. 46 (2017) 3060–3094.
[2] J.A. Pereira, A.M. Pessoa, M.N.D.S. Cordeiro, R. Fernandes, C. Prudêncio, J.P. Noronha, M. Vieira, Quinoxaline, its derivatives and applications: a state of the art review, Eur. J. Med. Chem. 97 (2015) 664–672.
[3] V.A. Mamedov, Quinoxalines: Synthesis, Reactions, Mechanisms and Structure, Springer, Cham, 2016.
[4] A. Rashidizadeh, H. Ghafuri, H. Reza, E. Zand, N. Goodarzi, Graphitic carbon nitride nanosheets covalently functionalized with biocompatible vitamin B1: synthesis, characterization, and its superior performance for synthesis of quinoxalines, ACS Omega 4 (2019) 12544–12554.
[5] C. Xie, Z. Zhang, B. Yang, G. Song, H. Gao, L. Wen, C. Ma, An efficient iodine-DMSO catalyzed synthesis of quinoxaline derivatives, Tetrahedron 71 (2015) 1831–1837.
[6] R.P. Pandit, H. Kim, Y. Rok, Iron-catalyzed annulation of 1,2-diamines and diazodicarbonyls for diverse and polyfunctionalized quinoxalines, pyrazines, and benzoquinoxalines in water, Adv. Synth. Catal. 358 (2016) 3586–3599.
[7] M. Inoue, S. Kamiguchi, K. Ugawa, S. Hkiri, J. Bouffard, D. Sémeril, T. Iwasawa, Evaluation of the catalytic capability of *cis*- and *trans*- diquinoxaline spanned cavitands, Eur. J. Org. Chem. 2019 (2019) 6261–6268.
[8] M. Torelli, I. Domenichelli, A. Pedrini, F. Guagnini, R. Pinalli, F. Terenziani, F. Artoni, R. Brighenti, E. Dalcanale, pH-driven conformational switching of quinoxaline cavitands in polymer matrices, Synlett 29 (2018) 2503–2508.
[9] F. Xie, M. Zhang, H. Jiang, M. Chen, W. Lv, A. Zheng, X. Jian, Efficient synthesis of quinoxalines from 2-nitroanilines and vicinal diols *via* a ruthenium-catalyzed hydrogen transfer strategy, Green Chem. 17 (2015) 279–284.
[10] D. Panja, B. Paul, B. Balasubramaniam, R.K. Gupta, S. Kundu, Application of a reusable Co-based nanocatalyst in alcohol dehydrogenative coupling strategy: synthesis of quinoxaline and imine scaffolds, Catal. Commun. 137 (2020) 105927.
[11] D. Wang, D. Astruc, The golden age of transfer hydrogenation, Chem. Rev. 115 (2015) 6621–6686.
[12] V.H. Mai, G.I. Nikonov, Transfer hydrogenation of nitriles, olefins, and N–heterocycles catalyzed by an N–heterocyclic carbene-supported half-sandwich complex of ruthenium, Organometallics 35 (2016) 943–949.
[13] C. Romain, S. Gaillard, M.K. Elmkaddem, L. Toupet, C. Fischmeister, C.M. Thomas, J.L. Renaud, New dipyridylamine ruthenium complexes for transfer hydrogenation of aryl ketones in water, Organometallics 29 (2010) 1992–1995.
[14] F.E. Fernández, M.C. Puerta, P. Valerga, Ruthenium(II) picolyl-NHC complexes: synthesis, characterization, and catalytic activity in amine N–alkylation and transfer hydrogenation reactions, Organometallics 31 (2012) 6868–6879.
[15] B. Xiong, J. Jiang, S. Zhang, H. Jiang, Z. Ke, M. Zhang, Ruthenium-catalyzed direct synthesis of semisaturated bicyclic pyrimidines *via* selective transfer hydrogenation, Org. Lett. 19 (2017) 2730–2733.
[16] P. Sharma, J. Rathod, A.P. Singh, P. Kumar, Y. Sasson, Synthesis of heterogeneous Ru(II)-1,2,3-triazole catalyst supported over SBA-15: application to the hydrogen transfer reaction and unusual highly selective 1,4-disbustituted traizole formation *via* multicomponent click reaction, Catal. Sci. Technol. 8 (2018) 3246–3259.
[17] J. Kim, C.S. Yi, Intermolecular Markovnikov-selective hydroacylation of olefins catalyzed by a cationic ruthenium−hydride complex, ACS Catal. 6 (2016) 3336–3339.
[18] A.D. Dwivedi, V.K. Sahu, S.M. Mobin, S.K. Singh, Cyclopentadienyl−Ru(II)−pyridylamine complexes: Synthesis, X–ray structure, and application in catalytic transformation of bio-derived furans to levulinic acid and diketones in water, Inorg. Chem. 57 (2018) 4777–4787.
[19] M. Kaloğlu, N. Gürbüz, D. Sémeril, I. Özdemir, Ruthenium(II)-(*p*-cymene)-N-heterocyclic carbene complexes for the N-alkylation of amine using the green hydrogen borrowing methodology, Eur. J. Inorg. Chem. 2018 (2018) 1236–1243.
[20] P. Kumar, R.K. Gupta, D.S. Pandey, Half-sandwich arene ruthenium complexes: synthetic strategies and relevance in catalysis, Chem. Soc. Rev. 43 (2014) 707–733.
[21] E. Manrique, I. Ferrer, C. Lu, X. Fontrodona, M. Rodríguez, I. Romero, A heterogeneous ruthenium DMSO complex supported onto silica particles as a recyclable catalyst for the efficient hydration of nitriles in aqueous medium, Inorg. Chem. 58 (2019) 8460–8470.
[22] R.K. Sharma, S. Dutta, S. Sharma, Quinoline-2-carboimine copper complex immobilized on amine functionalized silica coated magnetite nanoparticles: a novel and magnetically retrievable catalyst for the synthesis of carbamates *via* C–H activation of formamides, Dalton Trans. 44 (2015) 1303–1316.
[23] R.K. Sharma, S. Sharma, S. Dutta, R. Zboril, M.B. Gawande, Silica–nanosphere-based organic–inorganic hybrid nanomaterials: synthesis, functionalization and applications in catalysis, Green Chem. 17 (2015) 3207–3230.
[24] M. Khan, M.N. Tahir, S.F. Adil, H.U. Khan, M.R.H. Siddiqui, A.A. Al-Warthan, W. Tremel, Graphene-based metal and metal oxide nanocomposites: synthesis, properties and their applications, J. Mater. Chem. A 3 (2015) 18753–18808.
[25] B.F. MacHado, P. Serp, Graphene-based materials for catalysis, Catal. Sci. Technol. 2 (2012) 54–75.
[26] X. Fan, G. Zhang, F. Zhang, Multiple roles of graphene in heterogeneous catalysis, Chem. Soc. Rev. 44 (2015) 3023–3035.
[27] Y. Cheng, Y. Fan, Y. Pei, M. Qiao, Graphene-supported metal/metal oxide nanohybrids: synthesis and applications in heterogeneous catalysis, Catal. Sci. Technol. 5 (2015) 3903–3916.
[28] N.M. Julkapli, S. Bagheri, Graphene-supported heterogeneous catalysts: an overview, Int. J. Hydrogen Energy 40 (2015) 948–979.
[29] J. Pyun, Graphene oxide as catalyst: application of carbon materials beyond nanotechnology, Angew. Chem. Int. Ed. 50 (2011) 46–48.
[30] H. Su, Z. Li, Q. Huo, J. Guan, Q. Kan, Immobilization of transition metal (Fe^{2+}, Co^{2+}, VO^{2+} or Cu^{2+}) Schiff base complexes onto graphene oxide as efficient and recyclable catalysts for epoxidation of styrene, RSC Adv. 4 (2014) 9990–9996.
[31] S. Diyarbakir, H. Can, Ö. Metin, Reduced graphene oxide-supported CuPd alloy nanoparticles as efficient catalysts for the Sonogashira cross-coupling reactions, ACS Appl. Mater. Interfaces 7 (2015) 3199–3206.
[32] Q. Zhao, Y. Zhu, Z. Sun, Y. Li, G. Zhang, F. Zhang, X. Fan, Combining palladium complex and organic amine on graphene oxide for promoted Tsuji–Trost allylation, J. Mater. Chem. A 3 (2015) 2609–2616.
[33] Q. Zhao, D. Chen, Y. Li, G. Zhang, F. Zhang, X. Fan, Rhodium complex immobilized on graphene oxide as an efficient and recyclable catalyst for hydrogenation of cyclohexene, Nanoscale 5 (2013) 882–885.
[34] C. Bai, Q. Zhao, Y. Li, G. Zhang, F. Zhang, X. Fan, Palladium complex immobilized on graphene oxide as an efficient and recyclable catalyst for Suzuki coupling reaction, Catal. Lett. 144 (2014) 1617–1623.
[35] S. Sabater, J.A. Mata, E. Peris, Catalyst enhancement and recyclability by immobilization of metal complexes onto graphene surface by noncovalent interactions, ACS Catal 4 (2014) 2038–2047.
[36] M. Gopiraman, I.S. Kim, I.M. Chung, Stepwise construction of Ru(II) center containing chiral thiourea ligand on graphene oxide: first efficient, reusable, and stable catalyst for asymmetric transfer hydrogenation of ketones, Catalysts 10 (2020) 175.
[37] D. Sindhuja, P. Vasanthakumar, N.S.P. Bhuvanesh, R. Karvembu, An acylthiourea ligated Fe(II) complex on silica nanoparticles for transfer hydrogenation of carbonyl compounds, Ind. Eng. Chem. Res. 57 (2018) 14386–14393.
[38] D. Sindhuja, P. Vasanthakumar, N.S.P. Bhuvanesh, R. Karvembu, Catalytic assessment of copper(I) complexes and a polymer analog towards the one-pot synthesis of imines and quinoxalines, Eur. J. Inorg. Chem. 2019 (31) (2019) 3588–3596.
[39] W.S. Hummers, J.R.E. Offemann, Preparation of graphitic oxide, J. Am. Chem. Soc. 80 (1958) 1339.
[40] S. Swaminathan, J. Haribabu, N.K. Kalagatur, R. Konakanchi, N. Balakrishnan, N. Bhuvanesh, R. Karvembu, Synthesis and anticancer activity of [$RuCl_2(\eta^6$–arene)(aroylthiourea)] complexes - high activity against the human neuroblastoma (IMR- 32) cancer cell line, ACS Omega 4 (2019) 6245–6256.
[41] K. Jeyalakshmi, J. Haribabu, C. Balachandran, E. Narmatha, N.S.P. Bhuvanesh, S. Aoki, S. Awale, R. Karvembu, Synthesis of Ru(II)-benzene complexes containing aroylthiourea ligand, and their binding with biomolecules and *in vitro* cytotoxicity through apoptosis, New J. Chem. 43 (2019) 3188-3198.
[42] P.N. Sathishkumar, N. Raveendran, N.S.P. Bhuvanesh, R. Karvembu, Chemoselective transfer hydrogenation of nitroarenes, ketones and aldehydes using acylthiourea-based Ru(II)(*p*-cymene) complexes as precatalysts, J. Organomet. Chem. 876 (2018) 57–65.
[43] B. Vellaichamy, P. Periakaruppan, A facile, one-pot and eco-friendly synthesis of gold/silver nanobimetallics smartened rGO for enhanced catalytic reduction of hexavalent chromium, RSC Adv. 6 (2016) 57380–57388.
[44] Z. Li, S. Wu, H. Ding, D. Zheng, J. Hu, X. Wang, Q. Huo, J. Guan, Q. Kan, Dioxomolybdenum(VI) complex covalently attached to amino-modified graphene oxide: heterogeneous catalyst for the epoxidation of alkenes, New J. Chem. 37 (2013) 1561–1568.
[45] C. Wu, F. Irshad, M. Luo, Y. Zhao, X. Ma, S. Wang, Ruthenium complexes immobilized on an azolium-based metal organic framework for highly efficient conversion of CO_2 into formic acid, ChemCatChem 11 (2019) 1256–1263.
[46] N. Shah, E. Gravel, D.V. Jawale, E. Doris, Carbon nanotube–gold nanohybrid catalyzed N- formylation of amines by using aqueous formaldehyde, ChemCatChem 7 (2015) 57–61.